Optics Letters

Functional *in vivo* imaging using fluorescence lifetime light-sheet microscopy

Claire A. Mitchell,[1] Simon P. Poland,[2,3] James Seyforth,[4] Jakub Nedbal,[2,3] Thomas Gelot,[5] Tahiyat Huq,[4] Gerhard Holst,[6] Robert D. Knight,[1,†] and Simon M. Ameer-Beg[2,4,*,†]

[1]Craniofacial Development and Stem Cell Biology, Guy's Campus, King's College London, London, UK
[2]Division of Cancer Studies, Guy's Campus, King's College London, London, UK
[3]Randall Division of Cell and Molecular Biophysics, Guy's Campus, King's College London, London, UK
[4]Department of Physics, Strand Campus, King's College London, London, UK
[5]Photonlines (France) Ltd., Saint-Germain-en-Laye, France
[6]Science & Research, PCO AG, Kelheim, Germany
*Corresponding author: simon.ameer-beg@kcl.ac.uk

Received 31 January 2017; revised 24 February 2017; accepted 24 February 2017; posted 27 February 2017 (Doc. ID 284998); published 23 March 2017

Light-sheet microscopy has become an indispensable tool for fast, low phototoxicity volumetric imaging of biological samples, predominantly providing structural or analyte concentration data in its standard format. Fluorescence lifetime imaging microscopy (FLIM) provides functional contrast, but often at limited acquisition speeds and with complex implementation. Therefore, we incorporate a dedicated frequency domain CMOS FLIM camera and intensity-modulated laser into a light-sheet setup to add fluorescence lifetime imaging functionality, allowing the rapid acquisition of volumetric data with concentration independent contrast. We then apply the system to image live transgenic zebrafish, demonstrating the capacity to rapidly collect volumetric FLIM data from an *in vivo* sample.

OCIS codes: (110.0180) Microscopy; (170.3650) Lifetime-based sensing; (180.2520) Fluorescence microscopy; (180.6900) Three-dimensional microscopy.

https://doi.org/10.1364/OL.42.001269

Many important outstanding questions in biology require the imaging of molecular dynamics at high spatial and temporal resolution *in vivo*. Light-sheet microscopy, or selective plane illumination microscopy (SPIM), has been developed over the past decade to become the method of choice for fast, low photobleaching imaging of many different biological samples, particularly *in vivo* [1].

Fluorescence lifetime imaging microscopy (FLIM) is an important method for achieving concentration independent contrast in cell biology [2–4]. In particular, time-domain FLIM, using the time-correlated single-photon counting (TCSPC) technique, represents the gold standard for measurement of molecular dynamic interactions using FRET methodology [5]. However, the accuracy of the measured lifetime is photon-number dependent, and TCSPC-FLIM is therefore an inherently slow process, even when multiplexed over many detectors [6]. This is incompatible with the need to measure lifetime signals in rapidly moving cells in parallel, *in vivo*, such as cancer or immune cells, which often move at speeds of the order of 10–50 $\mu m\,min^{-1}$ (e.g., [7]).

Frequency domain (FD)-FLIM can increase the acquisition speed above conventional photon counting methods, but is limited in lifetime accuracy by the applied modulation frequency [8]. However, if the expected lifetime of the sample is known and the modulation frequency is appropriately matched, FD-FLIM is the optimum choice for integration with wide-field microscopes [9], of which only light-sheets can provide fast, optically sectioned images.

In this Letter, we incorporate a CMOS camera (pco.flim [10], PCO AG) and modulated diode laser into a digitally scanned light-sheet microscope (DSLM) setup. In this way, we combine the speed of DSLM for 3D imaging with the functional information obtained from FD-FLIM.

Previous implementations of fluorescence lifetime imaging in a light-sheet microscope configuration have been described in Greger *et al.* [11] and Weber *et al.* [12], to image a MDCK cyst and cell spheroids, respectively. Both studies used a cylindrical lens generated light-sheet, combined with a gated image intensifier (GII) in their setups. The digitally scanned sheet used in this Letter is less prone to shadowing and readily convertible from the standard Gaussian sheet to other sheet generating mechanisms such as the Airy [13] or lattice light-sheet [14] or the inclusion of two-photon illumination [15]. GII cameras may also suffer from low light throughput and well-known artifacts such as photo-bleaching and image distortion [16–19]. The pco.flim, by contrast, switches between two charge collection taps at the modulation frequency so, ideally, every photon incident on a pixel is detected, increasing the collection efficiency compared to a GII.

A schematic of the FL-DSLM system is shown in Fig. 1. Briefly, the output from a fiber-coupled 488 nm modulated

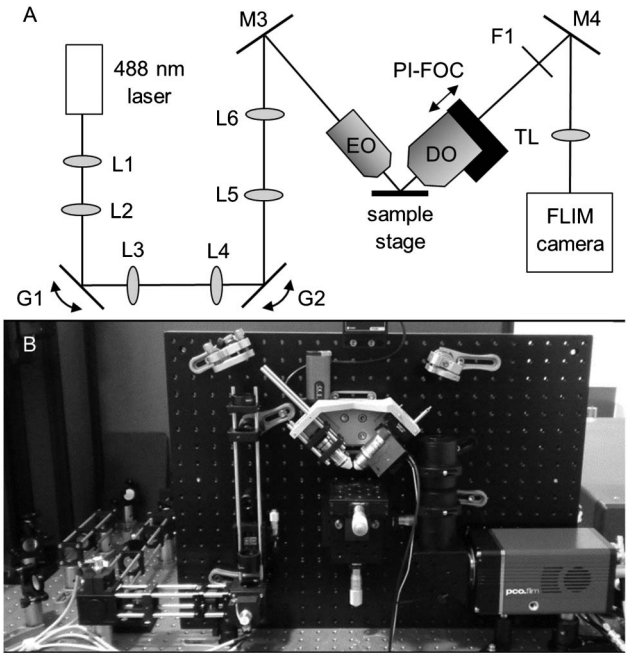

Fig. 1. Optical design of the FL-DSLM system as (A) a schematic and (B) photograph. From (A), the laser is magnified (L1 = 75 mm, L2 = 50 mm) and passed through a 4f scan system (L3, L4 = 50 mm) to create the light-sheet (G1) and provide z-movement (G2, coupled with the PI-FOC). The beam was then magnified 4× (L5 = 50 mm, L6 = 200 mm) and entered the EO to illuminate the sample. The emitted fluorescence was collected by the DO, band-pass filtered (F1) to remove any scattered excitation light and focused onto the FLIM camera using a tube lens (TL = 200 mm).

laser (PhoxX+ for pco.flim, Omicron–Laserage Laserprodukte GmbH, Germany) is directed into a galvanometer scanning system composed of two scanning mirrors separated by a 4f relay telescope. The beam is then magnified 4× before being conjugated onto the back of the excitation objective (EO) (10× water dipping, 0.3 NA, Nikon), ensuring the beam is stationary on the back focal plane. The objective back aperture is slightly underfilled to produce a focused scanned sheet with a depth-of-field of 100 μm, perpendicular to the detection objective (DO) focus (20× water dipping, 0.5 NA, Nikon). The generated fluorescence passes through an emission filter (540/50 nm, Semrock Inc., NY, U.S.) and is focused using a tube lens onto the pco.flim camera. Therefore, the pixel size is 280 nm, ensuring Nyquist sampling (theoretical resolution = 627 nm). The axial position of the DO is controlled using a piezo drive (PI-FOC, Physik Instrument GmbH, Germany), which is synchronized to the z-galvo to enable volumetric sweeps of the sample.

The system was controlled using software developed in LabVIEW. To collect FLIM images, the camera and laser were square wave modulated at 40 MHz; 16 images at equally spaced phase offsets between the camera and the laser trigger were obtained for each DSLM slice (covering one full modulation period) before moving to the next slice. Acquired images were analyzed in MATLAB (MathWorks, Inc., MA, U.S.). Briefly, lifetime values were extracted voxel-wise by applying an FFT to extract the phase (φ) and modulation depth (m) from sample images and a highly scattering LUDOX (Sigma-Aldrich Ltd., UK) reference

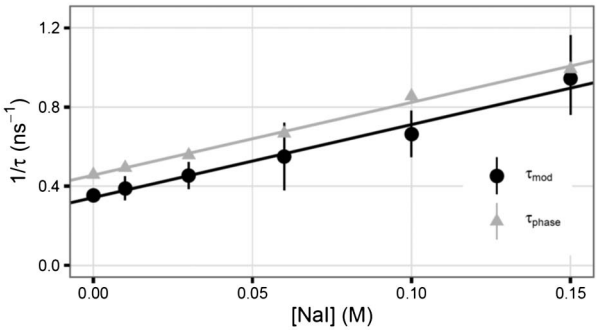

Fig. 2. Quantification of a FL-SPIM system. Upon addition of a quencher, sodium iodide, the lifetime (modulation in black, phase in gray) of a fluorescent lake of FITC decreases according to the Stern–Volmer equation. The error bars denote standard deviation ($n = 5$).

(φ_{ref}, m_{ref}). The phase and modulation lifetimes (τ_φ and τ_m, respectively) are calculated using Eqs. (1) and (2), where f is the applied modulation frequency [18]:

$$\tau_\varphi = \frac{1}{2\pi f}\tan((\varphi - \varphi_{\mathrm{ref}}) + \tan^{-1}(2\pi f \tau_{\mathrm{ref}})), \quad (1)$$

$$\tau_{\mathrm{mod}} = \frac{1}{2\pi f}\left(\frac{m_{\mathrm{ref}}^2}{m^2} - 1\right)^{1/2}. \quad (2)$$

Quantification of the system as a fluorescence lifetime microscope was performed by imaging fluorescein isothiocyanate (FITC, Sigma-Aldrich Ltd., UK) dissolved in PBS with increasing concentrations of quencher (NaI, Sigma-Aldrich Ltd., UK). The results are shown in Fig. 2.

The Stern–Volmer equation Eq. (3) describes a linear change in inverse lifetime (τ) upon the addition of a quenching agent at a concentration of $[Q]$ [20]:

$$1/\tau = k[Q] + 1/\tau_0. \quad (3)$$

This linear change is observed in Fig. 2 with fitted values of the bimolecular constant k calculated to be 3.67 and 3.76 $\mathrm{ns^{-1}\,M^{-1}}$ and t_0 of 2.17 and 2.94 ns using the calculated phase and modulation, respectively. The measured lifetime is shorter than the published value of 4.0 ns [20], but was consistent with data obtained on a multiphoton TCSPC microscope [21]. This shorter lifetime, coupled with a higher measured bimolecular constant (expected to be 2 $\mathrm{ns^{-1}\,M^{-1}}$ [20]) may be due to a low ionic strength FITC solution [22].

The lifetime calculated using the modulation shows a larger variance than the phase-based lifetime calculation. The modulation lifetime accuracy could be improved by applying the corrections described in Chen *et al.* [23].

After calibration of the lifetime, the system was able to measure relative phases in lifetime (Fig. 2). The system was then applied to an *in vivo* system: zebrafish (*danio rerio*). Two transgenic fish lines were used in this Letter: NFKB:EGFP [24] and α-actin:EGFP [25], both of which can be observed expressed in muscle fibers.

Fish were reared under standard conditions [26] as per UK Home Office regulations. In the case of the NFKB:EGFP fish, the larvae were injected with 20 $\mu g \cdot \mu l^{-1}$ 2 MDa FITC-dextran 24 h preceding imaging to perfuse the vasculature. At five days post-fertilization (dpf), larvae were embedded in low-melt

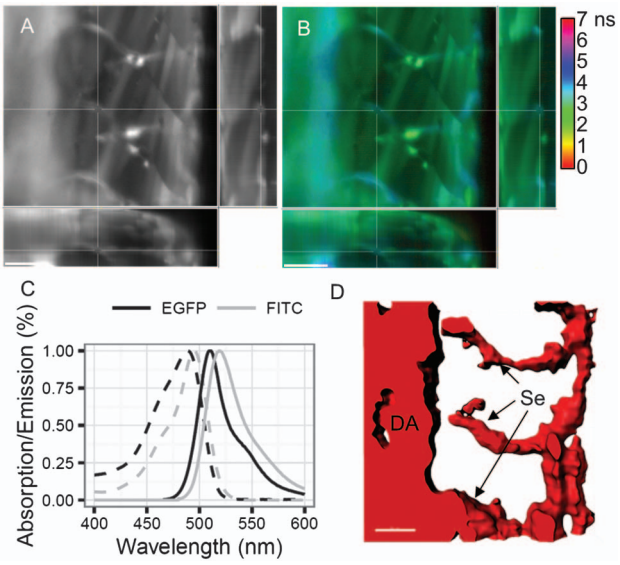

Fig. 3. FL-DSLM imaging of 5 dpf NFKB:EGFP zebrafish larvae. The camera exposure time was 1 s with 1 μm slice resolution. Extended orthogonal maximum projections (10 μm) of (A) the intensity and (B) the lifetime (both have a gamma correction of 0.5 applied) highlight the change in lifetime between the GFP muscle and FITC vasculature, despite the only small variation in color. The white lines denote the center of the displayed projections. (C) Absorption (dashed line) and emission (solid line) spectra of EGFP (black) and FITC (gray). (D) Segmented volume outlining the FITC-labelled vasculature, the dorsal aorta (DA) and intersegmental vessels (Se) can be clearly identified. The scale bar is 50 μm.

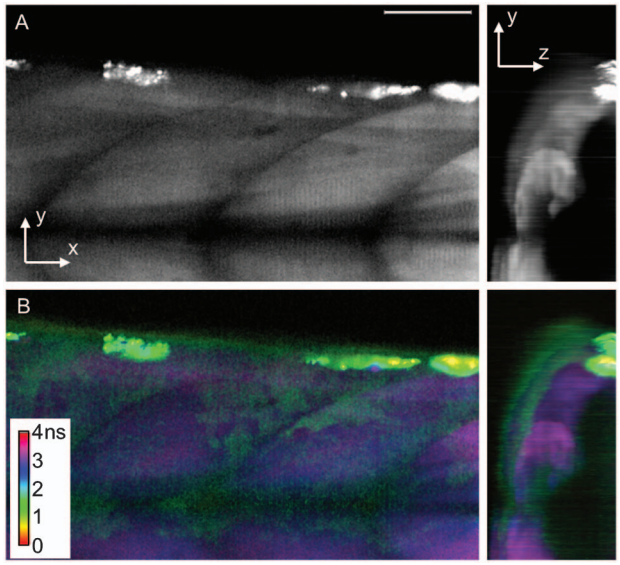

Fig. 4. FL-DSLM volume of α-actin:GFP zebrafish muscle collected with 200 ms exposure at 1 μm intervals. Maximum intensity projections of stack in the *xy* (left) and *yz* (right) planes for (A) the intensity and (B) the lifetime. The short lifetime of the autofluorescence on the skin can be distinguished from the long lifetime GFP (purple) expressed in the muscle. Green intensity has been artificially brightened slightly to highlight the thin skin layer against the bright EGFP signal. The scale bar is 50 μm.

agarose (Sigma-Aldrich Ltd.) in plastic 60 mm dishes (Nunc, Sigma-Aldrich Ltd.) with the dorsoventral axis at 45° to the base of the dish to optimally expose the muscle to the DO and immersed in an E3 medium with 0.01% MS-222 (Sigma-Aldrich Ltd.) and imaged immediately. Fluorescence lifetimes were calculated using Eq. (1). Intensity and intensity-mediated lifetime stacks were generated in MATLAB, and post-processing was performed in Imaris (Bitplane AG, Switzerland).

Images of the NFKB:EGFP and α-actin:EGFP fish are displayed in Figs. 3 and 4, respectively. In Fig. 3(B), the vasculature labelled in FITC-dextran ($\tau_{expected} = 4.0$ ns [20], $\tau_{measured} \sim 3.5$ ns) can be clearly discriminated from the EGFP-labelled ($\tau_{expected} = 2.4$ ns [27], $\tau_{measured} \sim 2.6$ ns) muscle by their different lifetimes, which is almost impossible by use of the intensity image only. [Figure 3(B) can only be seen where the FITC intensity is at its brightest.] This type of optical barcoding is useful to image fluorophores with similar emission wavelengths [Fig. 3(C)]. The dorsal aorta and intersegmental vessels can then be segmented from the phase lifetime image [Fig. 3(D), threshold = 2.9 ns] and appear as expected in a 5 dpf larvae [28].

Figure 3 was imaged using a long (1 s) camera exposure to remove FLIM artifacts introduced by the fast-moving blood cells. To show fast volumetric FLIM imaging, we therefore imaged α-actin:EGFP fish which expresses strongly in all the muscle fibers (Fig. 4). The volume displayed in Fig. 4 (280 μm × 280 μm × 100 μm before cropping) was collected in less than 7 min which is comparable to a commercial multiphoton or confocal system, but additionally capturing lifetime information.

Skin autofluorescence across a breadth of wavelengths presents a confounding factor when imaging transgenic zebrafish larvae in intensity-based approaches [29]. Utilizing FLIM, the short lifetime autofluorescence can easily be distinguished from the longer lifetime EGFP (Fig. 4).

In summary, we have presented the first *in vivo* demonstration of FL-DSLM using commercial FD-FLIM-enabled components. Using this system, we have been able to demonstrate fast volumetric FLIM imaging of zebrafish larvae muscle and to distinguish between spectrally similar fluorophores, using their different lifetimes.

The deployment of a digitally scanned light-sheet opens the options for beam shaping for improved field-of-view and resolution. The speed of acquisition could also be improved further by decreasing the number of phases acquired, potentially reaching speeds of up to 10 s per volume [30]. Such speeds of acquisition, coupled with low phototoxicity of the light-sheet microscope, make this configuration suitable for probing lifetime signals from rapidly moving cells *in vivo*.

Funding. Wellcome Trust (101529/Z/13/Z, 108111/Z/15/Z); Biotechnology and Biological Sciences Research Council (BBSRC) (BB/IAA/KCL/15, BB/L015773/1, BB/M015300/1); Cancer Research UK; Engineering and Physical Sciences Research Council (EPSRC); Medical Research Council (MRC); Department of Health (DH).

Acknowledgment. The authors thank David Gibson of Photon Lines Ltd. for the loan of the camera and laser.

†These authors contributed equally to this Letter.

REFERENCES

1. J. Huisken, J. Swoger, F. Del Bene, J. Wittbrodt, and E. H. K. Stelzer, Science **305**, 1007 (2004).
2. J. A. Levitt, D. R. Matthews, S. M. Ameer-Beg, and K. Suhling, Curr. Opin. Biotechnol. **20**, 28 (2009).
3. K. Suhling, L. M. Hirvonen, J. A. Levitt, P.-H. Chung, C. Tregidgo, A. Le Marois, D. A. Rusakov, K. Zheng, S. Ameer-Beg, S. Poland, S. Coehlo, R. Henderson, and N. Krstajić, Med. Photon., **27**, 3 (2015).
4. P. I. H. Bastiaens and A. Squire, Trends Cell Biol. **9**, 48 (1999).
5. G. O. Fruhwirth, L. P. Fernandes, G. Weitsman, G. Patel, M. Kelleher, K. Lawler, A. Brock, S. P. Poland, D. R. Matthews, G. Kéri, P. R. Barber, B. Vojnovic, S. M. Ameer-Beg, A. C. C. Coolen, and F. Fraternali, ChemPhysChem. **12**, 442 (2011).
6. S. P. Poland, N. Krstajić, J. Moneypenny, S. Coehlo, D. Tyndall, R. J. Walker, V. Devauges, J. Richardson, N. Dutton, P. Barber, D. D.-U. Li, K. Suhling, T. Ng, R. K. Henderson, and S. M. Ameer-Beg, Biomed. Opt. Express **6**, 277 (2015).
7. R. A. Ream, J. A. Theriot, and G. N. Somero, J. Exp. Biol. **206**, 4539 (2003).
8. A. Leray, F. B. Riquet, E. Richard, C. Spriet, D. Trinel, and L. He, Microsc. Res. Tech. **72**, 371 (2009).
9. R. M. Clegg, O. Holub, and C. Gohlke, Methods Enzymol. **360**, 509 (2003).
10. R. Franke and G. A. Holst, Proc. SPIE **9328**, 93281K (2015).
11. K. Greger, M. J. Neetz, E. G. Reynaud, and E. H. K. Stelzer, Opt. Express **19**, 20743 (2011).
12. P. Weber, S. Schickinger, M. Wagner, B. Angres, T. Bruns, and H. Schneckenburger, Int. J. Mol. Sci. **16**, 5375 (2015).
13. T. Vettenburg, H. I. C. Dalgarno, J. Nylk, C. Coll-Lladó, D. E. K. Ferrier, T. Čižmár, F. J. Gunn-Moore, and K. Dholakia, Nat. Methods **11**, 541 (2014).
14. B.-C. Chen, W. R. Legant, K. Wang, L. Shao, D. E. Milkie, M. W. Davidson, C. Janetopoulos, X. S. Wu, J. A. Hammer III, Z. Liu, B. P. English, Y. Mimori-Kiyosue, D. P. Romero, A. T. Ritter, J. Lippincott-Schwartz, L. Fritz-Laylin, R. Dyche Mullins, D. M. Mitchell, J. N. Bembenek, A.-C. Reymann, R. Böhme, S. W. Grill, J. T. Wang, G. Seydoux, U. Serdar Tulu, D. P. Kiehart, and E. Betzig, Science **346**, 6208 (2014).
15. T. V. Truong, W. Supatto, D. S. Koos, J. M. Choi, and S. E. Fraser, Nat. Methods **8**, 757 (2011).
16. Q. S. Hanley, V. Subramaniam, D. J. Arndt-Jovin, and T. M. Jovin, Cytometry A **43**, 248 (2001).
17. E. B. van Munster and T. W. Gadella, Jr., J. Microsc. **213**, 29 (2004).
18. E. B. van Munster and T. W. Gadella, Jr., Cytometry A **58**, 185 (2004).
19. M. vandeVen, M. Ameloot, B. Valeur, and N. Boens, J. Fluoresc. **15**, 377 (2005).
20. D. M. Jameson, *Introduction to Fluorescence* (Taylor & Francis, 2014).
21. T. Kiuchi, E. Ortiz-Zapater, J. Monypenny, D. R. Matthews, L. K. Nguyen, J. Barbeau, O. Coban, K. Lawler, B. Burford, D. J. Rolfe, E. de Rinaldis, D. Dafou, M. A. Simpson, N. Woodman, S. Pinder, C. E. Gillett, V. Devauges, S. P. Poland, G. Fruhwirth, P. Marra, Y. L. Boersma, A. Plückthun, W. J. Gullick, Y. Yarden, G. Santis, M. Winn, B. N. Kholodenko, M. L. Martin-Fernandez, P. Parker, A. Tutt, S. M. Ameer-Beg, and T. Ng, Sci. Signal **7**, ra78 (2014).
22. R. W. Stoughton and G. K. Rollefson, J. Am. Chem. Soc. **61**, 2634 (1939).
23. H. Chen, G. Holst, and E. Gratton, Microsc. Res. Tech. **78**, 1075 (2015).
24. M. Kanther, X. Sun, M. Mühlbauer, L. C. Mackey, E. J. Flynn III, M. Bagnat, C. Jobin, and J. F. Rawls, Gastroenterology **141**, 197 (2011).
25. S. Higashijima, H. Okamoto, N. Ueno, Y. Hotta, and G. Eguchi, Dev. Biol. **192**, F2 (1997).
26. M. Westerfield, *The Zebrafish Book: A Guide for Laboratory Use of the Zebrafish Danio Rerio* (University of Oregon, 2007).
27. R. Pepperkok, A. Squire, S. Geley, and P. I. H. Bastiaens, Curr. Biol. **9**, 269 (1999).
28. S. Isogai, M. Horiguchi, and B. M. Weinstein, Dev. Biol. **230**, 278 (2001).
29. J. Karlsson, J. von Hofsten, and P.-E. Olsson, Mar. Biotechnol. **3**, 0522 (2001).
30. M. Raspe, K. M. Kedziora, B. van den Broek, Q. Zhao, S. de Jong, J. Herz, M. Mastop, J. Goedhart, T. W. Gadella, Jr., I. T. Young, and K. Jalink, Nat. Methods **13**, 501 (2016).